The SUMO E3 Ligase SIZ1 Positively Regulates Active DNA Demethylation by Stabilizing ROS1 in *Arabidopsis thaliana*

Xiangfeng Kong[1,2,#], Yechun Hong[1,2,#], Yi-Feng Hsu[1], Huan Huang[1], Jian-Kang Zhu[1,3,*]

[1]Shanghai Center for Plant Stress Biology and Center for Excellence in Molecular Plant Sciences, Chinese Academy of Sciences, Shanghai 200032, People's Republic of China

[2]University of Chinese Academy of Sciences, Beijing, People's Republic of China

[3]Department of Horticulture and Landscape Architecture, Purdue University, West Lafayette, Indiana 47907, USA

[*]Correspondence: Jian-Kang Zhu, jkzhu@sibs.ac.cn

[#]These authors contributed equally to this work

Running title: SIZ1 Promotes DNA Demethylation by Stabilizing ROS1

Abstract

The 5-methylcytosine DNA glycosylase/lyase REPRESSOR OF SILENCING 1 (ROS1)-mediated active DNA demethylation is critical for shaping the genomic DNA methylation landscape in *Arabidopsis*. Whether and how the stability of ROS1 may be regulated by post-translational modifications is unknown. Using a methylation-sensitive PCR (CHOP-PCR)-based forward genetic screen for *Arabidopsis* DNA hypermethylation mutants, we identified the SUMO E3 ligase SIZ1 as a critical regulator of active DNA demethylation. Dysfunction of SIZ1 leads to hyper-methylation at approximately 1,400 genomic regions. SIZ1 physically interacts with ROS1 and mediates the SUMOylation of ROS1. The SUMOylation of ROS1 is reduced in *siz1* mutant plants. Compared to that in wild type plants, the protein level of ROS1 is significantly decreased, even though there is an increased level of *ROS1* transcripts in *siz1* mutant plants. Our results suggest that SIZ1 positively regulates

active DNA demethylation by promoting the stability of ROS1 protein through SUMOylation.

Introduction

As an important and conserved epigenetic marks, 5-methylcytosine DNA methylation takes part in various biological processes such as genomic imprinting, paramutation, X chromosome inactivation, and transcriptional gene silencing of transgene as well as endogenous gene (Baulcombe, 2004; Chandler and Stam, 2004; He *et al*., 2011; Heard, 2004; Scott and Spielman, 2004). In mammals, methylated cytosine is mainly at the CG context, while in plants cytosine methylation occurs in all sequence contexts (CG, CHG, and CHH, H represents for A, T and G). In plants, the DNA methylation is established *de novo* via the RNA-directed DNA methylation (RdDM) pathway, in which the DNA methyltransferase DRM2 is recruited to specific loci through the base-paring interactions between 24 nt siRNAs produced by the plant specific RNA polymerase pol IV and nascent long noncoding RNAs transcribed by another plant specific RNA polymerase, pol V (Law and Jacobsen, 2010; Matzke and Mosher, 2014; Pikaard *et al*., 2012; Zhang *et al*., 2018; Zhang and Zhu, 2012). Once been established, DNA methylation is maintained by specific mechanisms according to the sequence context. MET1 and CMT3 are responsible for maintaining DNA methylation at symmetric CG and CHG contexts, respectively (Law and Jacobsen, 2010). The CHH methylation is maintained by DRM2 through the RdDM pathway and by CMT2 (Zemach *et al*., 2013).

DNA methylation is reversible and its levels are determined by both the DNA methylation and demethylation processes. DNA demethylation can be passive and active (Zhu, 2009). The *Arabidopsis* 5-methylcytosine DNA glycosylase/lyase ROS1 is critical for pruning DNA methylation to keep a proper DNA methylation pattern genome-wide (Gong *et al*., 2002; Qian *et al*., 2012). The recruitment of ROS1 to specific genomic loci requires the Increased DNA Methylation (IDM) complex to

catalyze histone acetylations, which in turn attact the SWR1 complex for the deposition of H2A.Z required for the direct recruitment of ROS1 (Lang *et al*., 2015; Li *et al*., 2015; Li *et al*., 2012; Nie *et al*., 2019; Qian *et al*., 2012; Wang *et al*., 2015). ROS1 belongs to a small family of enzymes that also includes DME, DML2 and DML3 (Zhu, 2009), which are iron-sulfur proteins requiring Fe-S clusters as cofactors for enzymatic activities (Balk and Pilon, 2011; Netz *et al*., 2014). A cytosolic iron-sulfur assembly (CIA) pathway component, MET18, is required for delivery of Fe-S clusters to ROS1, and is thus important for the enzymatic activity of ROS1 (Duan *et al*., 2015; Wang *et al*., 2016). Little is known about whether and how ROS1 may be regulated by post-translational modifications.

Mechanistically similar to ubiquitination, SUMOylation occurs through an enzyme cascade (Seeler and Dejean, 2003). A maturation process is needed for the nascently synthesized SUMO protein, where the precursor protein is cleaved by a family of SUMO proteases SENPs/Ulps to exposure the C-terminal Gly-Gly motif that is indispensable for SUMO conjugation to its substrates (Mukhopadhyay and Dasso, 2007). In *Arabidopsis*, the mature forms of SUMOs are subsequently activated by a heterodimeric E1 activating enzyme (SAE1/SAE2) in an ATP-dependent way, then transferred to an E2 conjugating enzyme (SCE1), and finally covalently conjugated to the specific lysine residues of substrate proteins (Augustine and Vierstra, 2018). The SUMO E3 ligase can facilitate SUMO conjugation by E2 to the substrates, and can increase the substrate specificity (Gareau and Lima, 2010; Johnson, 2004). In yeast and metazoans, SUMOylation has been observed to regulate innate immunity, chromatin stability, gene transcription, DNA base excision repair and subcellular localization of target proteins (Gill, 2005; Johnson, 2004). In *Arabidopsis*, the dysfunction of SUMO E3 ligase SIZ1 is reported to affect ABA responses, cold tolerance, flowering time, basal thermotolerance, phosphate starvation responses, salicylic acid (SA)-dependent defense responses and photomorphogenesis (Lin *et al*., 2016; Lois *et al*., 2003; Mazur *et al*., 2019; Miura *et al*., 2007a; Miura *et al*., 2007b; Miura *et al*., 2009; Miura *et al*., 2005).

Here, we show that SIZ1 positively regulates active DNA demethylation mainly through a ROS1-dependent pathway. Mutation of *SIZ1* leads to a genome-wide hyper-methylation phenotype similar to that in *ros1* mutants. We found that SIZ1 directly interacts with ROS1 and facilitates the SUMO modification of ROS1. Dysfunction of SIZ1 causes defects in ROS1 SUMOylation and a reduction in ROS1 protein level. Our study reveals an important connection between SUMOylation and active DNA demethylation in plants.

Results

SIZ1 positively regulates active DNA demethylation independently of SA

To identify candidate genes involved in active DNA demethylation, we screened for transferred DNA (T-DNA) insertion mutants of *Arabidopsis thaliana* with a DNA hyper-methylation phenotype at the 3' region of *At1g26400* by CHOP-PCR as previously described (Qian *et al*., 2012). Two mutants bearing T-DNA insertion in the SUMO E3 ligase gene *SIZ1* (SALK_065397/*siz1-2* and SALK_034008/*siz1-3*) showed a hyper-methylation phenotype (Fig. 1A and S1A). Locus-specific bisulfite sequencing result of the 3' region of *At1g26400* indicated that in *ros1-4*, *siz1-2* and *siz1-3*, the methylation levels increased in all sequence contexts (i.e. CG, CHG and CHH. Fig. 1B). CHOP-PCR test on another 3 loci (*At1g26390*, *At1g26410* and *At4g18650*) known as ROS1 target loci was performed on *siz1* mutants (Fig. 1C). The results indicated that the *siz1* mutations cause hyper-methylation at these 3 loci. Locus-specific bisulfite sequencing test confirmed the CHOP-PCR results (Fig. 1D). Methylation analysis of the *siz1-2 ros1-4* double mutant revealed that the hyper-methylation phenotypes of *siz1-2* and *ros1-4* are not additive (Fig. 1B and 1D), suggesting that SIZ1 and ROS1 may function in the same genetic pathway for active DNA demethylation.

SIZ1 contains five important domains such as the SAP domain, PHD domain, PINIT

domain, SP-RING domain and SXS motif. By introducing wild-type *SIZ1* and *SIZ1* alelles containing mutation disrupting each of these five domains into *siz1-2* to generate $SIZ1^{WT}$, $SIZ1^{sap}$, $SIZ1^{phd}$, $SIZ1^{pinit}$, $SIZ1^{sp\text{-}ring}$ and $SIZ1^{sxs}$ plants, Cheong and colleagues showed the specific domains of SIZ1 control unique responses to different environmental stimuli (Cheong *et al*., 2009). To examine the function of the various domains of SIZ1 in regulating active DNA demethylation, we analyzed the $SIZ1^{WT}$, $SIZ1^{sap}$, $SIZ1^{phd}$, $SIZ1^{pinit}$, $SIZ1^{sp\text{-}ring}$ and $SIZ1^{sxs}$ plants. CHOP-PCR results showed that expression of the wild type form but not any of the mutant forms of SIZ1 could rescue the hyper-methylation phenotype of *siz1-2* (Fig. S1B), demonstrating that all of these five domains are important for SIZ1 to regulate DNA demethylation at the 3' region of *At1g26400*.

Dysfunction of SIZ1 leads to an obvious dwarf phenotype due to the elevated salicylic acid (SA) level, which can be suppressed by introducing nahG, a salicylate hydroxylase from bacteria (Lee *et al*., 2007). To examine if the highly accumulated SA in *siz1*-2 mutant plants causes the hyper-methylation phenotype, we introduced the *nahG* gene into *siz1-2* mutant plants. The expression of *nahG* rescued the dwarf phenotype of *siz1-2* (Fig. S2A) but did not affect the DNA hyper-methylation phenotype (Fig. S2B), indicating that the hyper-methylation phenotype of *siz1-2* is not due to the elevated SA.

The indispensable role of SUMOylation in plant viability makes it impossible to use the knock-out mutants of key genes in the SUMOylation pathway. Homozygous mutants deficient in *SUMO1/2*, SUMO E1 activating enzyme subunit *SAE2* or SUMO E2 conjugating enzyme *SCE1* are embryonic lethal (Saracco *et al*., 2007). Over-expressing a mutated form of SCE1 containing the C94S substitution results in a dominant-negative effect, which impairs the SUMOylation process as previously reported (Tomanov *et al*., 2013). Therefore, to determine whether other SUMOylation pathway components may affect active DNA demethylation, we generated SCE(WT)-Flag and SCE(C94S)-Flag over-expression lines. The expression of

SCE(WT)-Flag and SCE(C94S)-Flag was confirmed by Western blot analysis (Fig. S3A). As reported by Tomanov and colleagues (Tomanov *et al*., 2013), the plants over-expressing SCE(C94S) showed a dwarf phenotype which is similar to *siz1* mutants (Fig. S3B). SCE(C94S)-Flag over-expressing plants showed DNA hyper-methylation at the 3' region of *At1g26400* similarly to *siz1* mutants, but the DNA hyper-methylation phenothype was not displayed by SCE(WT)-Flag over-expressing plants (Fig. S3C), demonstrating that proper SUMOylation is important for active DNA demethylation.

SIZ1 prevents DNA hyper-methylation at over a thousand genomic regions

According to whole genome bisulfite sequencing data, 3,757 differentially methylated regions (DMRs) were identified in *siz1-2* mutant plants. Among these, 1,489 were hyper-DMRs showing a significantly increased DNA methylation (Fig. 2A). About 40% of the hyper-DMRs identified in *siz1-2* mutant plants were overlapped with those in *ros1-4* mutant plants, indicating that SIZ1 may function by regulating ROS1 at these genomic regions. The composition of the hyper-DMRs identified in *siz1-2* mutant plants is similar to that in *ros1-4* mutant plants and very different from that of *ibm1-4* (Fig. 2B), which is a mutant defective in a histone H3K9 methyltransferase critical for preventing CHG methylation in gene body regions (Lei *et al*., 2014; Saze *et al*., 2008; Wang *et al*., 2013). Heatmap analysis also showed that the DNA methylation pattern especially in the CG context in *siz1-2* is more similar to those in *ros1-4* and *rdd* (a triple mutant defective in *ROS1* and its paralogs *DML2* and *DML3*) than to that in *ibm1-4* (Fig. 2C). These results suggested that SIZ1 positively regulates active DNA demethylation mainly at ROS1 target loci.

SIZ1 physically interacts with ROS1

To examine if SIZ1 may physically interact with ROS1, yeast two-hybrid (Y2H) assays were performed. The full-length coding sequences of *SIZ1* and *ROS1* were amplified and cloned into pGAD-T7 and pGBK-T7 vectors, respectively. Only yeast cells carrying both SIZ1-AD and ROS1-BD grew well on the SD-Leu/-Trp/-His/-Ade

media and turned blue with the supplement of X-α-Gal (Fig. 3A), indicating that SIZ1 interacts with ROS1 in yeast. The direct interaction between SIZ1 and ROS1 was confirmed by split-LUC and bimolecular fluorescence complementation (BiFC) assays in *Nicotiana benthamiana* leaves. In the split-LUC assay, strong LUC signals were detected only cLUC-SIZ1 and ROS1-nLUC were co-expressed (Fig. 3B). The BiFC results showed a YFP fluorescence signal in the nucleus of *Nicotiana benthamiana* cells co-expressing SIZ1 fused with C-terminal region of YFP and ROS1 fused with N-terminal region of YFP (Fig. 3C), suggesting that SIZ1 interacts with ROS1 in the nucleus. Additionally, HA-SIZ1 could be co-immunoprecipitated with ROS1-Flag (Fig. 3D) when they are co-expressed in *Arabidopsis* protoplasts, which further confirmed the interaction between SIZ1 and ROS1. These results showed that SIZ1 physically interacts with ROS1 in the nucleus.

SIZ1 enhances the SUMOylation of ROS1

The interaction between SIZ1 and ROS1 further prompted us to test whether ROS1 may be SUMOylated. SUMOylation site prediction by SUMOplot (http://www.abgent.com/sumoplot) and GPS-SUMO (http://sumosp.biocuckoo.org) suggested that there are five possible SUMOylation sites in the ROS1 protein (Fig. S4), which indicated that ROS1 may be a target of SUMOylation. To examine the possibility of ROS1 as a SUMO modification target, we firstly tested the interaction between SUMO1 and ROS1 by the split-LUC assay in *Nicotiana benthamiana* leaves (Fig. 4A). The results indicated that ROS1 interacts with SUMO1 via a region located in the C-terminus of ROS1 (ROS1b, 510-1393 aa) which contains the DNA glycosylase and CTD domains. The interactions between SUMO1 with two ROS1 paralologs, DML2 and DML3, were also tested in the same assay, which did not show any interaction, indicating that SUMO1 specifically interacts with ROS1. Next, to analyze whether ROS1 is SUMOylated, we performed an *in vitro* SUMOylation assay as previously described (Okada *et al*., 2009). Based on the localization of SUMOylation sites, two truncated ROS1 containing predicted SUMOylation sites, ROS1c (1-290 aa, containing one predicted SUMOylation site: K133) and ROS1d

(794-1063 aa, containing four predicted SUMOylation sites: K806/K812/K851/K1051), were generated and expressed with the fusion of a T7 tag. Immunoblot analysis showed that a shift of protein band to higher molecular weight was observed in crude lysates from *E.coli* BL21(DE3) cells expressing ROS1d but not ROS1c together with SUMO E1 (SAE1b and SAE2), SUMO E2 (SCE1) and the mature form SUMO1 (SUMO1GG) (Fig. 4B). A similar result was obtained when T7-ROS1c/ROS1d was replaced with GST-ROS1c/ROS1d-Myc (Fig. S5) in the assay. The resutls suggested that ROS1 can be SUMOylated *in vitro*, and the SUMOylation is mainly in the DNA glycosylase domain.

To determine the SUMO modification of ROS1 *in vivo* in plant cells, we co-expressed ROS1-Flag and ROS1b-Flag with HA-SUMO1 in Col-0 protoplasts. A shift of protein band to higher molecular weight was detected when ROS1-Flag or ROS1b-Flag was co-expressed with HA-SUMO1, but not in protoplasts expressing HA-SUMO1 only, suggesting that ROS1 was SUMOylated in *vivo*, and the SUMOylation likely happens within the DNA glycosylase (Fig. 4C). To determine the role of SIZ1 on SUMOylation of ROS1, we conducted the *in vivo* SUMOylation assay by co-expressing ROS1-Flag with HA-SUMO1 in Col-0 and *siz1-2* protoplasts. A strong and clear band corresponding to SUMO1-modified ROS1 was detected in Col-0 protoplasts. A substantially weaker band was detected in *siz1-2* protoplasts (Fig. 4D). These results indicate that ROS1 is SUMOylated by SUMO1 *in vivo*, and that SIZ1 enhances the SUMO1 modification of ROS1. We used LC-MS/MS to analyze the protein band showing mobility shift, and the result confirmed ROS1 is SUMO1 modified (Fig. S6). The remaining SUMO1 modified ROS1 in *siz1-2* mutant protoplasts may due to the basal modification by E1/E2, independently of SIZ1, which is consistent with the *in vitro* SUMOylation assay showing that ROS1 could be SUMOylated without an E3 ligase (Fig. 4B). SUMOylation can occur without E3 ligases in some cases, although the substrate range and extent of SUMOylation *in vivo* is determined by SUMO E3 ligases (Bernier-Villamor *et al*., 2002; Meulmeester *et al*., 2008; Zhu *et al*., 2008). The lysine to arginine substitution can block the

SUMOylation on substrate proteins (Gostissa *et al*., 1999). We co-expressed ROS1(5K/Rs)-Flag with all the 5 predicted SUMOylation sites mutated by lysine to arginine substitutions together with HA-SUMO1 in Col-0 protoplasts. The SUMO1 modification of ROS1 was blocked by these 5 lysine to arginine substitutions (Fig. 4D), demonstrating that ROS1 is SUMOylated at one or more of these 5 predicted lysines.

The protein level of ROS1 is reduced in *siz1* mutant plants

SUMOylation is known as an important post-translational modification regulating the stability of substrate proteins (Hay, 2005). Since SIZ1 mediates the SUMOylation of ROS1 (Fig. 4, S5 and S6), and positively regulates active DNA demethylation in many genomic regions targeted by ROS1 (Fig. 1 and 2), we speculated that SIZ1-mediated SUMOylation may promote active DNA demethylation by enhancing the stability of ROS1. To test this hypothesis, the protein level of ROS1 in *siz1-2* mutant plants was detected by Western blot analysis. We crossed *siz1-2* mutant plants to a *GFP* knock-in line with *GFP* inserted in and fused in-frame with the endogenous *ROS1* in Col-0 (*ROS1-GFP*/Col-0) (Miki *et al*., 2018), and obtained *ROS1-GFP*/*siz1-2* plants. Immunodetection of ROS1-GFP protein level by anti-GFP antibodies showed that the ROS1-GFP protein was substantially deceased in *siz1-2* mutant plants (Fig. 5).

To exclude the possibility that the reduced ROS1 protein level in *siz1* mutant plants may be due to a lower transcript level of *ROS1*, RT-qPCR was performed to determine the *ROS1* transcript level in *siz1* mutant plants. Interestingly, the results showed that dysfunction of SIZ1 led to a significantly increased *ROS1* transcript level compared to that in Col-0 (Fig. S7A). The *ROS1-GFP* transcript level was also not lower in *ROS1-GFP*/*siz1-2* plants compared to that in *ROS1-GFP*/Col-0 plants (Fig. S7B). Together, these results support that SIZ1 enhances the stability of ROS1 by facilitating the SUMOylation of ROS1.

Discussion

In recent years, several studies have elucidated the mechanisms of ROS1 targeting and activity regulation. The newly discovered IDM complex functions together with the SWR1 complex in recruiting ROS1 to specific genomic loci for active DNA demethylation (Duan *et al*., 2017; Lang *et al*., 2015; Li *et al*., 2015; Nie *et al*., 2019; Qian *et al*., 2014; Qian *et al*., 2012; Wang *et al*., 2015). MET18 is critical for the regulation of enzymatic activity of ROS1 (Duan *et al*., 2015; Wang *et al*., 2016). However, whether and how the stability of ROS1 may be regulated have not been investigated. Our findings suggest that the SUMO E3 ligase SIZ1 has a critical role in enhancing the stability of ROS1 via facilitating the SUMOylation of ROS1.

Effects of SUMOylation on DNA methylation in *Arabidopsis*

Similar to that in *ros1-4* mutant, *siz1* mutants and plants over-expressing dominant-negative SUMO E2 SCE(C94S) showed a DNA hyper-methylation phenotype which is independent of SA accumulation (Fig. 1, S1B, S2 and S3). The hyper-DMRs in *siz1-2* are highly overlapped with those in *ros1-4* or *rdd* (Fig. 2), and the hyper-methylation phenotypes of *siz1-2* and *ros1-4* are not additive (Fig. 1B and 1D). These observations suggest that SIZ1 positively regulates active DNA demethylation at genomic regions targeted by the ROS1 family of 5-methylcytosine DNA glycoslase/lyases.

The role of SUMO modification in active DNA demethylation has been reported in mammals (McLaughlin *et al*., 2016; Steinacher *et al*., 2019; Waters *et al*., 1999). SUMO modification is important for orchestrating the thymine deaminase TDG-initiated base excision repair (BER) process required for active DNA demethylation (Steinacher *et al*., 2019). Recently, SUMOylation studies in plants indicated that some components of the RdDM pathway and BER pathway, as well as some DNA methyltransferases can be SUMOylated or interact with SUMO in *Arabidopsis* (Elrouby *et al*., 2013; Kim *et al*., 2015; Miller *et al*., 2010; Rytz *et al*.,

2018). Besides positive regulation of active DNA demethylation by facilitating the SUMOylation of ROS1 and other regulators of demethylation, SIZ1 may also regulate DNA methylation by facilitating the SUMOylation of DNA methyltransferases and other methylation regulators. This may explain the many hypo-DMRs that were also identified in *siz1* mutant plants.

Stability regulation of DNA glycosylase ROS1 by SUMO E3 ligase SIZ1

As a DNA glycosylase, ROS1 needs to be targeted to specific genomic regions to prune the DNA methylation (Lang *et al*., 2015; Li *et al*., 2015; Qian *et al*., 2014; Qian *et al*., 2012; Wang *et al*., 2015). The delivery of Fe-S clusters to the iron-sulfur binding motif of ROS1 by MET18 is critical for the enzymatic activity of ROS1 (Duan *et al*., 2015; Wang *et al*., 2016). The mechanism of ROS1 stability regulation has been elusive. TDG, the DNA glycosylase in mammals is SUMOylated to enhance its enzymatic turnover, leading to more efficient active DNA demethylation (McLaughlin *et al*., 2016; Waters *et al*., 1999). In this study, we showed that one of the DNA glycosylases in *Arabidopsis* ROS1 can also be SUMOylated, which is facilitated by SUMO E3 ligase SIZ1 (Fig. 4, S5 and S6). Our results indicate that the C-terminus of ROS1 containing the DNA glycosylase domain is required for the SUMOylation. Though the precise residues of SUMOylation site(s) remain to be determined, the blocking of SUMOylation by lysine to arginine substitutions in all five predicted sites confirmed the SUMO1 modification of ROS1. The *in vitro* and *in vivo* evidences all support that ROS1 is a SUMOylation substrate.

SUMOylation can affect the substrate proteins via regulation of protein stability, enzymatic activity, subcellular localization and protein-protein interactions (Hay, 2005). The protein level of ROS1 was examined in *siz1* mutant plants, and the Western-blotting result showed a reduced accumulation of ROS1 protein in *siz1-2* mutant plants (Fig. 5). The reduced ROS1 protein level was not due to decreased *ROS1* transcrit level in the mutant plants since an increased *ROS1* transcrit level was observed (Fig. S7A and S7B). Similar increases in *ROS1* transcript level have been

observed in mutant plants with defective active DNA demethylation, due to feedback regulation through the DNA methylation monitoring sequence at the *ROS1* gene promoter (Lei *et al*., 2015; Zheng *et al*., 2008).

There is still ROS1 protein accumulation in *siz1* mutant plants, athough the level is reduced. The remaining ROS1 protein may explain why not all ROS1 targeted genomic regions is affected in *siz1* mutants. SUMOylation can attenuate ubiquitin-mediated degradation process, and the possibility of ROS1 as a possible ubiquitination substrate has been suggested (Hay, 2005; Miura *et al*., 2007b; Ulrich, 2005). SUMOylation of ROS1 may competitively affect the ubiquitination of ROS1 to reduce its degradation. Future work will determine whether ROS1 is ubiquitinated and whether the ubiquitination is affected in *siz1* mutants. It will also be interesting to investigate whether the enzymatic turnover or activity of ROS1 may be regulated by SUMO modification.

Materials and Methods

Plant materials and isolation of mutants by CHOP-PCR

The *Arabidopsis siz1-2* (SALK_065397) and *siz1-3* (SALK_034008) mutant seeds *Arabidopsis* were obtained from the Arabidopsis Biological Resource Center (ABRC, http://www.arabidopsis.org). For generating SCE(WT) and SCE(C94S) over-expression lines, the coding sequence of *SCE1a* were amplified and cloned into pCAMBIA1305 vector to generate pCAMBIA1305-*35S:*SCE(WT)-3*Flag construct, and then this construct was used for mutagenesis to generate pCAMBIA1305-*35S:*SCE(C94S)-3*Flag construct. These two constructs were introduced to Col-0 plants through *Agrobacteria* using the floral dipping method (Clough and Bent, 1998), and the T3 homozygous lines were used for analysis. Seedlings were grown on 1/2 Murashige and Skoog (MS) agar plates containing 1 % (w/v) sucrose and 0.5 % (w/v) agar at 22 °C under 16 h light/8 h dark photoperiod for

2 weeks before DNA or RNA isolation. Plants including *Arabidopsis* and *Nicotiana benthamiana* were grown in soil at 23 °C under a 16 h light/8 h dark photoperiod.

Screening for mutants was as described (Qian *et al*., 2012). In brief, 500 ng of genomic DNA was digested by *HhaI* in a 20 μl reaction mixture. Two μl of digested DNA was used as template for PCR in a 20 μl reaction mixture using *At1g26400* primer. Primers are listed in Table S1.

Locus-specific bisulfite sequencing

One hundred ng of genomic DNA was treated by the BisulFlash DNA Modification Kit (Epigentek) following the manufacturer's protocol. One μl of bisulfite-treated DNA was used for PCR in 20 μl of reaction mixture using ExTag (Takara) with specific primers (Table S1). PCR products were cloned into the pMD-18T vector (Takara) following the manufacturer's instructions. For each locus in each sample, at least 15 independent top-strand clones were selected for sequencing and analysis.

Whole-genome bisulfite sequencing and data analysis

Fourteen-day-old seedlings were used for genomic DNA extraction using DNeasy Plant Kit (Qiagen) following the manufacturer's protocols. Bisulfite treatment, library construction, and deep sequencing were performed by the Genomics Core Facility at the Shanghai Center for Plant Stress Biology, China. Data analysis was conducted as previously reported (Nie *et al*., 2019).

Yeast two-hybrid assay

Yeast two-hybrid assay was carried out as described previously (Hong *et al*., 2020). The coding sequence of *ROS1* was fused in-frame with the GAL4 DNA binding domain (BD) of the bait vector pGBKT7 (Clontech). The coding sequence of *SIZ1* was cloned in-frame with the GAL4 activation domain (AD) of the prey vector pGADT7 (Clontech). Different combinations of bait and prey plasmids were co-transformed into the yeast strain AH109 (*Saccharomyces cerevisiae*). The

transformed yeast cells were grown on the –L/-W medium for selection for 3 days at 30 °C. The positive clones were spotted on –L/-W/-H/-A medium supplemented with or without X-α-gal followed by a 10^x series dilution.

Split-LUC assay

For detecting the interaction between SIZ1 and ROS1, the full-length coding sequences of *ROS1* and *SIZ1* were amplified and cloned into the pCAMBIA-nLUC and pCAMBIA-cLUC vectors, respectively. For analyzing the interaction between ROS1 and SUMO1, the full-length coding sequence of *SUMO1* was cloned into the pCAMBIA-cLUC vector to generate cLUC-SUMO1, and truncated ROS1 fragments such as ROS1a (1-509 aa) and ROS1b (510-1393 aa) were cloned into the pCAMBIA-nLUC vector to generate ROS1a-nLUC and ROS1b-nLUC. The recombinant plasmids were transformed into *Agrobacterium* stain GV3101. Different combinations of *Agrobacterium* GV3101 carrying different constructs were co-infiltrated into *Nicotiana benthamiana* leaves. After 48 h of incubation, the *Agrobacterium*-infiltrated leaves were infiltrated with 1 μM luciferin and allowed to incubate at dark for 10 min. The luminescence signal was detected by a low-light cooled CCD imaging system (Lumazone; Roper Scientific).

Bimolecular fluorescence complementation (BiFC) assay

The coding sequences of *SIZ1* and *ROS1* were amplified and cloned into p2YC vector and p2YN vector, respectively. The recombinant plasmids were transformed into *Agrobacterium* stain GV3101. Specific combinations of *Agrobacterium* GV3101 carrying different plasmids were co-infiltrated into *Nicotiana benthamiana* leaves. After an incubation for 36 h, and the YFP fluorescence signals were detected and photographed by a confocal laser-scanning microscope (Zeiss LSM880).

Co-Immunoprecipitation assay

The full-length coding sequences of *ROS1* and *SIZ1* were cloned into pUC18-Flag and pUC18-HA vectors, separately, for expression of ROS1-Flag and SIZ1-HA fusion

proteins. The *35S:ROS1-Flag* and *35S:SIZ1-HA* were co-expressed in Col-0 protoplasts by polyethylene glycol (PEG400)-mediated transformation as previously described (Yoo *et al*., 2007). The transformed protoplasts were incubated for 20 h at 22 °C. After incubation, the protoplasts were collected and lysed in 1 ml of 1 × protein extraction buffer (50 mM Tris-Cl (pH 7.5), 150 mM NaCl, 5 mM $MgCl_2$, 10% (v/v) glycerol, 0.1% (v/v) NP-40, 2 mM DTT, 1 mM PMSF, 1 × complete protease inhibitor mixture (Roche)). Fifty μl of anti-Flag mAb-Magnetic beads (MBL International) were added to the crude lysate supernatant and gently rotated for 2 h at 4 °C. The beads were then washed 5 times by 1 ml of 1 × protein extraction buffer. The immunoprecipitated proteins were detected by Western-blotting. Anti-HA antibody (Roche) was used for detection of SIZ1-HA and anti-Flag antibody (Sigma) was used for ROS1-Flag detection.

SUMOylation assay and mass spectrometry

The *in vitro* SUMOylation assay was performed as previously described (Okada *et al*., 2009). To construct the plasmids for expression of N-terminal T7-tagged variant ROS1, the coding sequences of truncated *ROS1* (ROS1c: 1-290 aa, ROS1d: 794-1063 aa) were cloned into pET28a vector (Novagen) to generate pET28a-ROS1c and pET28a-ROS1d. To construct the plasmids for expression of GST-ROS1c/ROS1d-Myc, the coding sequences of ROS1c and ROS1d were amplified by primers tagged with Myc and cloned into pGEX4T1 (Addgene) to generate pGEX4T1_ROS1c-Myc and pGEX4T1_ROS1d-Myc. Three plasmids including pCDFDuet-AtSUMO1(AA/GG)-AtSCE1a expressing N-terminal His-tagged AtSUMO1(AA/GG) and C-terminal S-tagged AtSCE1a, pACYCDuet-AtSAE1b-AtSAE2 expressing N-terminal His-tagged AtSAE1b and C-terminal S-tagged AtSAE2, together with pET28a-ROS1c/ROS1d or pGEX4T1_ROS1c/ROS1d-Myc were co-transformed into *E.coli* BL21(DE3). After induction with 0.2 mM IPTG for 12 h at 25 °C, cells were collected and boiled in 1 × SDS sample buffer at 100 °C for 10 min. Equal amounts of *E.coli* protein extracts were separated by SDS-PGAE followed by Western-blotting using anti-T7 antibody

(Abcam) or anti-Myc antibody (Millipore).

In vivo SUMOylation assay was conducted as described (Zheng *et al*., 2012).The coding sequences of full-length *ROS1* and truncated *ROS1* (ROS1b: 510-1393 aa) were cloned into pUC18-Flag vector to produce ROS1/ROS1b-Flag fusion proteins. To generate plasmids for transient expression of HA-SUMO1, the full-length coding sequence of *SUMO1* was cloned into pUC18-HA vector. The *35S:ROS1-Flag* or *35S:ROS1b-Flag* and *35S:HA-SUMO1* were co-expressed in Col-0 or *siz1-2* protoplasts using polyethylene glycol (PEG4000)-mediated transformation (Yoo *et al*., 2007). After 20 h of incubation at 22 °C, the protoplasts were collected and lysed by 1 ml of 1 × protein extraction buffer. Fifty μl of anti-Flag mAb-Magnetic beads (MBL International) were added to the supernatant of crude protein lysate and incubated for 2 h at 4 °C. Then, the beads were washed 5 times with 1 ml of 1 × protein extraction buffer, and proteins were detected by Western-blotting. Anti-HA antibody (Roche) was used for detection of ROS1/ROS1b-Flag-HA-SUMO1 conjugation proteins and HA-SUMO1 as input. Anti-Flag antibody (Sigma) was used for immunodetection of ROS1/ROS1b-Flag as a control.

For LC-MS/MS analysis, the anti-Flag mAb-Magnetic beads immunoprecipitated proteins were separated in SDS-PAGE gel followed by silver staining using Fast Silver Stain Kit (Beyotime). The bands of ROS1 and SUMOylated ROS1 were cut into pieces according to their molecular weights and used for LC-MS/MS analysis at BGI.

Protein extraction and Western-blotting

Total protein extracts from 14-day-old seedlings (0.3 g) were prepared as previously described (Li *et al*., 2006). Equal amount of proteins were separated by SDS-PAGE and the gel blots probed using anti-GFP antibody (Roche) or anti-Actin antibody (Abmart).

RNA extraction and Real-Time quantitative RT-PCR

Total RNA was extracted from 0.1 g of 14-day-old seedlings by TRIzol reagent (Invitrogen), and cDNAs were synthesized by reverse transcription using the iScript cDNA synthesis kit (Bio-Rad). All Real-Time quantitative RT-PCR were performed in a CFX96 Real-time system (Bio-Rad) using the ChamQ SYBR qPCR Master Mix (Vazyme) following the manufacturer's instructions. Three biological replicates were included in each test. *AtUBQ10* was used as an internal control. The primers used were listed in Table S1.

Accession numbers

Sequence data from this article can be found in The Arabidopsis Information Resource (http://www.arabidopsis.org/) under the following accession numbers: *SIZ1* (At5g60410), *ROS1* (At2g36490), *SUMO1* (At4g26840), *TUB8* (At5g23860), *UBQ10* (At4g05320), *SCE1* (At3g57870), *DML2* (At3g10010), *DML3* (At4g34060).

Supplemental Items

Supplemental Figure 1. Characterization of *SIZ1* T-DNA insertion mutants.

Supplemental Figure 2. Hyper-methylation caused by *siz1* mutation is not due to the elevated SA.

Supplemental Figure 3. Plants over-expressing dominant-negative SUMO E2 SCE(C94S) show DNA hypermethylation at *At1g26400* loci.

Supplemental Figure 4. Predicted SUMOylation sites in ROS1.

Supplemental Figure 5. ROS1 is SUMOylated.

Supplemental Figure 6. Detection of SUMOylated ROS1 by LC-MS/MS.

Supplemental Figure 7. *ROS1* expression level in the *siz1* mutants.

Supplemental Table 1. Primers used in this study.

Acknowledgements

We thank Dr. Katsunori Tanaka for kindly providing the constructs for SUMOylation test in *E.coli* (pCDFDuet-AtSUMO1(AA/GG)-AtSCE1a,

pACYCDuet-AtSAE1b-AtSAE2). Dr. Dae-Jin Yu for kindly providing the transgenic plants of *SIZ1* carrying point mutations at specific domains (SIZ1^{sap}, SIZ1^{phd}, SIZ1^{pinit}, SIZ1$^{sp\text{-}ring}$, SIZ1^{sxs}). Dr. Jie Zhang for her technical support. This work was supported by the Chinese Academy of Sciences to J.-K.Z.

Author contributions

Conception and design: Jian-Kang Zhu, Xiangfeng Kong, Yi-Feng Hsu

Performed research: Xiangfeng Kong, Yechun Hong

Methylome analysis: Huan Huang

Writing, review, and/or revision of the manuscript: Xiangfeng Kong, Jian-Kang Zhu, Yechun Hong

Conflict of interest

The authors declare no competing interests.

References

Augustine, R.C., and Vierstra, R.D. (2018). SUMOylation: re-wiring the plant nucleus during stress and development. Curr Opin Plant Biol *45*, 143-154.

Balk, J., and Pilon, M. (2011). Ancient and essential: the assembly of iron-sulfur clusters in plants. Trends Plant Sci *16*, 218-226.

Baulcombe, D. (2004). RNA silencing in plants. Nature *431*, 356-363.

Bernier-Villamor, V., Sampson, D.A., Matunis, M.J., and Lima, C.D. (2002). Structural basis for E2-mediated SUMO conjugation revealed by a complex between ubiquitin-conjugating enzyme Ubc9 and RanGAP1. Cell *108*, 345-356.

Chandler, V.L., and Stam, M. (2004). Chromatin conversations: mechanisms and implications of paramutation. Nat Rev Genet *5*, 532-544.

Cheong, M.S., Park, H.C., Hong, M.J., Lee, J., Choi, W., Jin, J.B., Bohnert, H.J., Lee, S.Y.,

Bressan, R.A., and Yun, D.J. (2009). Specific domain structures control abscisic acid-, salicylic acid-, and stress-mediated SIZ1 phenotypes. Plant Physiol *151*, 1930-1942.

Clough, S.J., and Bent, A.F. (1998). Floral dip: a simplified method for Agrobacterium-mediated transformation of Arabidopsis thaliana. Plant J *16*, 735-743.

Duan, C.G., Wang, X., Tang, K., Zhang, H., Mangrauthia, S.K., Lei, M., Hsu, C.C., Hou, Y.J., Wang, C., Li, Y.*, et al.* (2015). MET18 Connects the Cytosolic Iron-Sulfur Cluster Assembly Pathway to Active DNA Demethylation in Arabidopsis. PLoS Genet *11*, e1005559.

Duan, C.G., Wang, X., Xie, S., Pan, L., Miki, D., Tang, K., Hsu, C.C., Lei, M., Zhong, Y., Hou, Y.J.*, et al.* (2017). A pair of transposon-derived proteins function in a histone acetyltransferase complex for active DNA demethylation. Cell Res *27*, 226-240.

Elrouby, N., Bonequi, M.V., Porri, A., and Coupland, G. (2013). Identification of Arabidopsis SUMO-interacting proteins that regulate chromatin activity and developmental transitions. Proc Natl Acad Sci U S A *110*, 19956-19961.

Gareau, J.R., and Lima, C.D. (2010). The SUMO pathway: emerging mechanisms that shape specificity, conjugation and recognition. Nat Rev Mol Cell Biol *11*, 861-871.

Gill, G. (2005). Something about SUMO inhibits transcription. Curr Opin Genet Dev *15*, 536-541.

Gong, Z., Morales-Ruiz, T., Ariza, R.R., Roldan-Arjona, T., David, L., and Zhu, J.K. (2002). ROS1, a repressor of transcriptional gene silencing in Arabidopsis, encodes a DNA glycosylase/lyase. Cell *111*, 803-814.

Gostissa, M., Hengstermann, A., Fogal, V., Sandy, P., Schwarz, S.E., Scheffner, M., and Del Sal, G. (1999). Activation of p53 by conjugation to the ubiquitin-like protein SUMO-1. EMBO J

18, 6462-6471.

Hay, R.T. (2005). SUMO: a history of modification. Mol Cell *18*, 1-12.

He, X.J., Chen, T., and Zhu, J.K. (2011). Regulation and function of DNA methylation in plants and animals. Cell Res *21*, 442-465.

Heard, E. (2004). Recent advances in X-chromosome inactivation. Curr Opin Cell Biol *16*, 247-255.

Hong, Y., Wang, Z., Liu, X., Yao, J., Kong, X., Shi, H., and Zhu, J.-K. (2020). Two Chloroplast Proteins Negatively Regulate Plant Drought Resistance Through Separate Pathways. Plant Physiology.

Johnson, E.S. (2004). Protein modification by SUMO. Annu Rev Biochem *73*, 355-382.

Kim, D.Y., Han, Y.J., Kim, S.I., Song, J.T., and Seo, H.S. (2015). Arabidopsis CMT3 activity is positively regulated by AtSIZ1-mediated sumoylation. Plant Sci *239*, 209-215.

Lang, Z., Lei, M., Wang, X., Tang, K., Miki, D., Zhang, H., Mangrauthia, S.K., Liu, W., Nie, W., Ma, G.*, et al.* (2015). The methyl-CpG-binding protein MBD7 facilitates active DNA demethylation to limit DNA hyper-methylation and transcriptional gene silencing. Mol Cell *57*, 971-983.

Law, J.A., and Jacobsen, S.E. (2010). Establishing, maintaining and modifying DNA methylation patterns in plants and animals. Nat Rev Genet *11*, 204-220.

Lee, J., Nam, J., Park, H.C., Na, G., Miura, K., Jin, J.B., Yoo, C.Y., Baek, D., Kim, D.H., Jeong, J.C.*, et al.* (2007). Salicylic acid-mediated innate immunity in Arabidopsis is regulated by SIZ1 SUMO E3 ligase. Plant J *49*, 79-90.

Lei, M., La, H., Lu, K., Wang, P., Miki, D., Ren, Z., Duan, C.G., Wang, X., Tang, K., Zeng, L.*, et*

al. (2014). Arabidopsis EDM2 promotes IBM1 distal polyadenylation and regulates genome DNA methylation patterns. Proc Natl Acad Sci U S A *111*, 527-532.

Lei, M., Zhang, H., Julian, R., Tang, K., Xie, S., and Zhu, J.K. (2015). Regulatory link between DNA methylation and active demethylation in Arabidopsis. Proc Natl Acad Sci U S A *112*, 3553-3557.

Li, C.F., Pontes, O., El-Shami, M., Henderson, I.R., Bernatavichute, Y.V., Chan, S.W., Lagrange, T., Pikaard, C.S., and Jacobsen, S.E. (2006). An ARGONAUTE4-containing nuclear processing center colocalized with Cajal bodies in Arabidopsis thaliana. Cell *126*, 93-106.

Li, Q., Wang, X., Sun, H., Zeng, J., Cao, Z., Li, Y., and Qian, W. (2015). Regulation of Active DNA Demethylation by a Methyl-CpG-Binding Domain Protein in Arabidopsis thaliana. PLoS Genet *11*, e1005210.

Li, X., Qian, W., Zhao, Y., Wang, C., Shen, J., Zhu, J.K., and Gong, Z. (2012). Antisilencing role of the RNA-directed DNA methylation pathway and a histone acetyltransferase in Arabidopsis. Proc Natl Acad Sci U S A *109*, 11425-11430.

Lin, X.L., Niu, D., Hu, Z.L., Kim, D.H., Jin, Y.H., Cai, B., Liu, P., Miura, K., Yun, D.J., Kim, W.Y., *et al.* (2016). An Arabidopsis SUMO E3 Ligase, SIZ1, Negatively Regulates Photomorphogenesis by Promoting COP1 Activity. PLoS Genet *12*, e1006016.

Lois, L.M., Lima, C.D., and Chua, N.H. (2003). Small ubiquitin-like modifier modulates abscisic acid signaling in Arabidopsis. Plant Cell *15*, 1347-1359.

Matzke, M.A., and Mosher, R.A. (2014). RNA-directed DNA methylation: an epigenetic pathway of increasing complexity. Nat Rev Genet *15*, 394-408.

Mazur, M.J., Kwaaitaal, M., Mateos, M.A., Maio, F., Kini, R.K., Prins, M., and van den Burg, H.A. (2019). The SUMO Conjugation Complex Self-Assembles into Nuclear Bodies Independent of SIZ1 and COP1. Plant Physiol *179*, 168-183.

McLaughlin, D., Coey, C.T., Yang, W.C., Drohat, A.C., and Matunis, M.J. (2016). Characterizing Requirements for Small Ubiquitin-like Modifier (SUMO) Modification and Binding on Base Excision Repair Activity of Thymine-DNA Glycosylase in Vivo. J Biol Chem *291*, 9014-9024.

Meulmeester, E., Kunze, M., Hsiao, H.H., Urlaub, H., and Melchior, F. (2008). Mechanism and consequences for paralog-specific sumoylation of ubiquitin-specific protease 25. Mol Cell *30*, 610-619.

Miki, D., Zhang, W., Zeng, W., Feng, Z., and Zhu, J.K. (2018). CRISPR/Cas9-mediated gene targeting in Arabidopsis using sequential transformation. Nat Commun *9*, 1967.

Miller, M.J., Barrett-Wilt, G.A., Hua, Z., and Vierstra, R.D. (2010). Proteomic analyses identify a diverse array of nuclear processes affected by small ubiquitin-like modifier conjugation in Arabidopsis. Proc Natl Acad Sci U S A *107*, 16512-16517.

Miura, K., Jin, J.B., and Hasegawa, P.M. (2007a). Sumoylation, a post-translational regulatory process in plants. Curr Opin Plant Biol *10*, 495-502.

Miura, K., Jin, J.B., Lee, J., Yoo, C.Y., Stirm, V., Miura, T., Ashworth, E.N., Bressan, R.A., Yun, D.J., and Hasegawa, P.M. (2007b). SIZ1-mediated sumoylation of ICE1 controls CBF3/DREB1A expression and freezing tolerance in Arabidopsis. Plant Cell *19*, 1403-1414.

Miura, K., Lee, J., Jin, J.B., Yoo, C.Y., Miura, T., and Hasegawa, P.M. (2009). Sumoylation of ABI5 by the Arabidopsis SUMO E3 ligase SIZ1 negatively regulates abscisic acid signaling.

Proc Natl Acad Sci U S A *106*, 5418-5423.

Miura, K., Rus, A., Sharkhuu, A., Yokoi, S., Karthikeyan, A.S., Raghothama, K.G., Baek, D., Koo, Y.D., Jin, J.B., Bressan, R.A.*, et al.* (2005). The Arabidopsis SUMO E3 ligase SIZ1 controls phosphate deficiency responses. Proc Natl Acad Sci U S A *102*, 7760-7765.

Mukhopadhyay, D., and Dasso, M. (2007). Modification in reverse: the SUMO proteases. Trends Biochem Sci *32*, 286-295.

Netz, D.J., Mascarenhas, J., Stehling, O., Pierik, A.J., and Lill, R. (2014). Maturation of cytosolic and nuclear iron-sulfur proteins. Trends Cell Biol *24*, 303-312.

Nie, W.F., Lei, M., Zhang, M., Tang, K., Huang, H., Zhang, C., Miki, D., Liu, P., Yang, Y., Wang, X.*, et al.* (2019). Histone acetylation recruits the SWR1 complex to regulate active DNA demethylation in Arabidopsis. Proc Natl Acad Sci U S A *116*, 16641-16650.

Okada, S., Nagabuchi, M., Takamura, Y., Nakagawa, T., Shinmyozu, K., Nakayama, J., and Tanaka, K. (2009). Reconstitution of Arabidopsis thaliana SUMO pathways in E. coli: functional evaluation of SUMO machinery proteins and mapping of SUMOylation sites by mass spectrometry. Plant Cell Physiol *50*, 1049-1061.

Pikaard, C.S., Haag, J.R., Pontes, O.M., Blevins, T., and Cocklin, R. (2012). A transcription fork model for Pol IV and Pol V-dependent RNA-directed DNA methylation. Cold Spring Harb Symp Quant Biol *77*, 205-212.

Qian, W., Miki, D., Lei, M., Zhu, X., Zhang, H., Liu, Y., Li, Y., Lang, Z., Wang, J., Tang, K.*, et al.* (2014). Regulation of active DNA demethylation by an alpha-crystallin domain protein in Arabidopsis. Mol Cell *55*, 361-371.

Qian, W., Miki, D., Zhang, H., Liu, Y., Zhang, X., Tang, K., Kan, Y., La, H., Li, X., Li, S.*, et al.*

(2012). A histone acetyltransferase regulates active DNA demethylation in Arabidopsis. Science *336*, 1445-1448.

Rytz, T.C., Miller, M.J., McLoughlin, F., Augustine, R.C., Marshall, R.S., Juan, Y.T., Charng, Y.Y., Scalf, M., Smith, L.M., and Vierstra, R.D. (2018). SUMOylome Profiling Reveals a Diverse Array of Nuclear Targets Modified by the SUMO Ligase SIZ1 during Heat Stress. Plant Cell *30*, 1077-1099.

Saracco, S.A., Miller, M.J., Kurepa, J., and Vierstra, R.D. (2007). Genetic analysis of SUMOylation in Arabidopsis: conjugation of SUMO1 and SUMO2 to nuclear proteins is essential. Plant Physiol *145*, 119-134.

Saze, H., Shiraishi, A., Miura, A., and Kakutani, T. (2008). Control of genic DNA methylation by a jmjC domain-containing protein in Arabidopsis thaliana. Science *319*, 462-465.

Scott, R.J., and Spielman, M. (2004). Epigenetics: imprinting in plants and mammals--the same but different? Curr Biol *14*, R201-203.

Seeler, J.S., and Dejean, A. (2003). Nuclear and unclear functions of SUMO. Nat Rev Mol Cell Biol *4*, 690-699.

Steinacher, R., Barekati, Z., Botev, P., Kusnierczyk, A., Slupphaug, G., and Schar, P. (2019). SUMOylation coordinates BERosome assembly in active DNA demethylation during cell differentiation. EMBO J *38*.

Tomanov, K., Hardtke, C., Budhiraja, R., Hermkes, R., Coupland, G., and Bachmair, A. (2013). Small ubiquitin-like modifier conjugating enzyme with active site mutation acts as dominant negative inhibitor of SUMO conjugation in arabidopsis(F). J Integr Plant Biol *55*, 75-82.

Ulrich, H.D. (2005). Mutual interactions between the SUMO and ubiquitin systems: a plea of

no contest. Trends Cell Biol *15*, 525-532.

Wang, C., Dong, X., Jin, D., Zhao, Y., Xie, S., Li, X., He, X., Lang, Z., Lai, J., Zhu, J.K., *et al.* (2015). Methyl-CpG-binding domain protein MBD7 is required for active DNA demethylation in Arabidopsis. Plant Physiol *167*, 905-914.

Wang, X., Duan, C.G., Tang, K., Wang, B., Zhang, H., Lei, M., Lu, K., Mangrauthia, S.K., Wang, P., Zhu, G., *et al.* (2013). RNA-binding protein regulates plant DNA methylation by controlling mRNA processing at the intronic heterochromatin-containing gene IBM1. Proc Natl Acad Sci U S A *110*, 15467-15472.

Wang, X., Li, Q., Yuan, W., Cao, Z., Qi, B., Kumar, S., Li, Y., and Qian, W. (2016). The cytosolic Fe-S cluster assembly component MET18 is required for the full enzymatic activity of ROS1 in active DNA demethylation. Sci Rep *6*, 26443.

Waters, T.R., Gallinari, P., Jiricny, J., and Swann, P.F. (1999). Human thymine DNA glycosylase binds to apurinic sites in DNA but is displaced by human apurinic endonuclease 1. J Biol Chem *274*, 67-74.

Yoo, S.D., Cho, Y.H., and Sheen, J. (2007). Arabidopsis mesophyll protoplasts: a versatile cell system for transient gene expression analysis. Nat Protoc *2*, 1565-1572.

Zemach, A., Kim, M.Y., Hsieh, P.H., Coleman-Derr, D., Eshed-Williams, L., Thao, K., Harmer, S.L., and Zilberman, D. (2013). The Arabidopsis nucleosome remodeler DDM1 allows DNA methyltransferases to access H1-containing heterochromatin. Cell *153*, 193-205.

Zhang, H., Lang, Z., and Zhu, J.K. (2018). Dynamics and function of DNA methylation in plants. Nat Rev Mol Cell Biol *19*, 489-506.

Zhang, H., and Zhu, J.K. (2012). Seeing the forest for the trees: a wide perspective on

RNA-directed DNA methylation. Genes Dev *26*, 1769-1773.

Zheng, X., Pontes, O., Zhu, J., Miki, D., Zhang, F., Li, W.X., Iida, K., Kapoor, A., Pikaard, C.S., and Zhu, J.K. (2008). ROS3 is an RNA-binding protein required for DNA demethylation in Arabidopsis. Nature *455*, 1259-1262.

Zheng, Y., Schumaker, K.S., and Guo, Y. (2012). Sumoylation of transcription factor MYB30 by the small ubiquitin-like modifier E3 ligase SIZ1 mediates abscisic acid response in Arabidopsis thaliana. Proc Natl Acad Sci U S A *109*, 12822-12827.

Zhu, J., Zhu, S., Guzzo, C.M., Ellis, N.A., Sung, K.S., Choi, C.Y., and Matunis, M.J. (2008). Small ubiquitin-related modifier (SUMO) binding determines substrate recognition and paralog-selective SUMO modification. J Biol Chem *283*, 29405-29415.

Zhu, J.K. (2009). Active DNA demethylation mediated by DNA glycosylases. Annual review of genetics *43*, 143-166.

Figure legends

Figure 1. The *siz1* mutant plants show DNA hyper-methylation at multiple loci. (A) Analysis of DNA methylation status at the 3' region of *At1g26400* by methylation-sensitive PCR (CHOP-PCR). Compared to that in wild type Col-0 plants, the methylation levels increased in *ros1-4*, *siz1-2* and *siz1-3* mutants. Undigested genomic DNA was used as a control. (B) Analysis of DNA methylation status at the 3' region of *At1g26400* via locus-specific bisulfite sequencing. (C) Analysis of DNA methylation status at multiple loci by CHOP-PCR. Similar to those in *ros1-4* mutant, the methylation levels increased at multiple loci in *siz1-2* and *siz1-3* mutants. (D) Analysis of DNA methylation status at the indicated loci via locus-specific bisulfite sequencing. The locus-specific bisulfite sequencing results confirmed the CHOP-PCR results.

Figure 2. *SIZ1* mutation causes genome-wide DNA hyper-methylation. (A) Numbers of hyper-DMRs identified in *siz1-2* mutant by whole-genome bisulfite sequencing, and the overlap with those in *ros1-4* mutant. (B) Genomic composition of hyper-DMRs in *siz1-2*, *ros1-4*, *idm1-1* and *ibm1-4* mutants. (C) Heat-map showing the methylation levels of *siz1-2* hyper-DMRs in the indicated mutants. The hyper-DMRs in different sequence contexts (CG, CHG or CHH) were analyzed.

Figure 3. SIZ1 physically interacts with ROS1. (A) Yeast two-hybrid result showing an interaction between SIZ1 and ROS1. Full-length SIZ1 and ROS1 were fused to AD and BD, respectively. The different combination of recombinant plasmids and empty vectors were co-transformed into yeast cells. AD, Gal4 activation domain; BD, Gal4 binding domain. (B) Split-LUC assay showing an interaction between SIZ1 and ROS1 in *Nicotiana benthamiana* leaves. The coding sequences of *SIZ1* and *ROS1* were fused to the C-terminal firefly luciferase and N-terminal firefly luciferase, respectively. (C) Bimolecular fluorescence complementation (BiFC) test indicating SIZ1 interaction with ROS1 in *Nicotiana benthamiana* leaves in the nucleus. Full-length SIZ1 and ROS1 were fused to the C-terminal YFP and N-terminal YFP, respectively. Chlorophyll, the autofluorescence of chlorophyll; BF, bright field; Scale bars, 20 μm. (D) Co-immunoprecipitation showing an association of SIZ1 with ROS1. HA-tagged SIZ1 and Flag-tagged ROS1 were expressed separately or co-expressed in *siz1-2* protoplasts. HA-SIZ1 and ROS1-Flag were detected by immuno-blotting using anti-HA and anti-Flag antibodies with crude lysate proteins and proteins immunoprecipitated via anti-Flag mAb-Magnetic beads, respectively.

Figure 4. SIZ1 mediates the SUMOylation of ROS1. (A) The interaction of SUMO1 and ROS1 was tested using the split-LUC assay. The C-terminal region of firefly luciferase was fused to the N-terminus of SUMO1. ROS1, DML2 and DML3 were fused to the N-terminal region of firefly luciferase. The schematic diagram shows the full-length ROS1 and the truncated ROS1 (ROS1a: 1-509 aa, ROS1b:

510-1393 aa). NTD, N-terminal domain; CTD, C-terminal domain. (B) SUMOylation of ROS1 was tested using the *Arabidopsis* SUMOylation pathway reconstitution system in *E.coli*. Different combinations of the three plasmids encoding *Arabidopsis* SUMOylation machinery proteins and truncated ROS1 indicated above each lane were co-transformed into *E.coli* BL21(DE3). Immuno-blotting was used to detect truncated ROS1 and its SUMOylated forms using anti-T7 antibody in crude lysate proteins. SUMOylated ROS1 shifting to a larger molecular weight band was observed only in the lane using the mature wild type form of SUMO1 (referred to as SUMO1GG), but not in lanes using mutated form of SUMO1 (referred to as SUMO1AA). The schematic diagram indicates the truncated ROS1 (ROS1c: 1-290 aa (containing K133), ROS1d: 794-1063 aa (containing K806. K812, K851 and K1051)). (C) *In vivo* SUMOylation of ROS1. ROS1-Flag/ROS1b-Flag and HA-SUMO1 were co-expressed in Col-0 protoplasts. The SUMOylated ROS1 was detected via immuno-blotting using anti-HA antibody in proteins immunoprecipitated by anti-Flag mAb-Magnetic beads. Expression of HA-SUMO1 with empty vector served as a negative control. (D) SUMOylation of ROS1 was reduced in *siz1-2*. ROS1-Flag/ROS1(5K/Rs)-Flag and HA-SUMO1 were co-expressed in Col-0 and *siz1-2* protoplasts. SUMOylation of ROS1 was substantially decreased in *siz1-2* compared to in Col-0. SUMOylation in mutant ROS1 with the 5 predicted SUMOylation sites mutated by lysine to arginine substitutions (K133R/K806R/K812R/K851R/K1051R) was reduced.

Figure 5. ROS1 protein level is decreased in *siz1-2* mutant plants. (A) Immunodetection of ROS1 protein level by anti-GFP antibody in *GFP* knock-in lines with *GFP* integrated in the endogenous *ROS1* locus in Col-0 and *siz1-2* background. Col-0 and *siz1-2* without the GFP served as negative controls. Actin detected by anti-Actin antibody was used as a loading control. The protein level of ROS1 relative to Actin shown above the lanes was quantified using Image Lab software (version 5.2.1). (B) Statistical analysis of the ROS1 protein level in *siz1-2* mutant (n=3). *P*

$= 0.0007 < 0.001$, determined by Student's t-test.

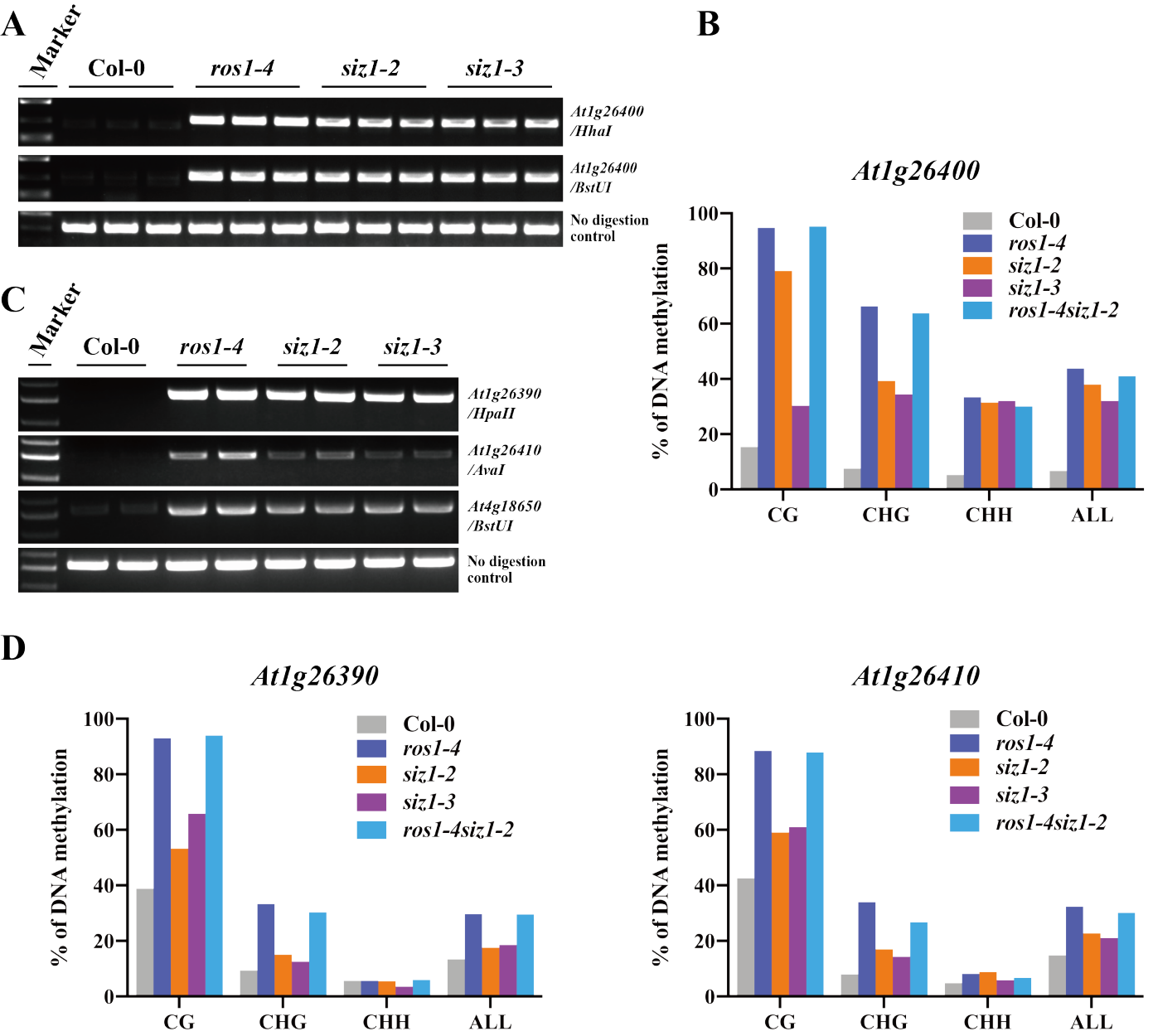

Figure 1. The *siz1* mutant plants show DNA hyper-methylation at multiple loci. (A) Analysis of DNA methylation status at the 3' region of *At1g26400* by methylation-sensitive PCR (CHOP-PCR). Compared to that in wild type Col-0 plants, the methylation levels increased in *ros1-4*, *siz1-2* and *siz1-3* mutants. Undigested genomic DNA was used as a control. (B) Analysis of DNA methylation status at the 3' region of *At1g26400* via locus-specific bisulfite sequencing. (C) Analysis of DNA methylation status at multiple loci by CHOP-PCR. Similar to those in *ros1-4* mutant, the methylation levels increased at multiple loci in *siz1-2* and *siz1-3* mutants. (D) Analysis of DNA methylation status at the indicated loci via locus-specific bisulfite sequencing. The locus-specific bisulfite sequencing results confirmed the CHOP-PCR results.

A

Hyper DMRs in *siz1-2*	Overlapped DMRs in *ros1-4*
1489	616(41.4%)

B

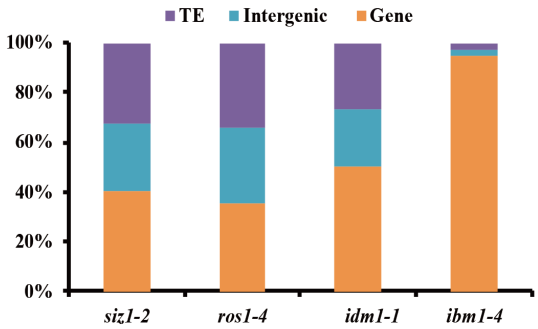

C

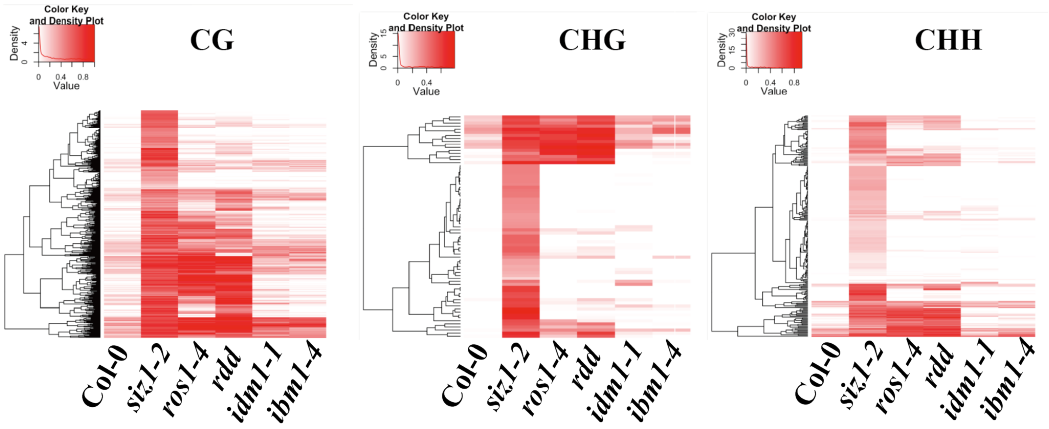

Figure 2. *SIZ1* mutation causes genome-wide DNA hyper-methylation. (A) Numbers of hyper-DMRs identified in *siz1-2* mutant by whole-genome bisulfite sequencing, and the overlap with those in *ros1-4* mutant. (B) Genomic composition of hyper-DMRs in *siz1-2*, *ros1-4*, *idm1-1* and *ibm1-4* mutants. (C) Heat-map showing the methylation levels of *siz1-2* hyper-DMRs in the indicated mutants. The hyper-DMRs in different sequence contexts (CG, CHG or CHH) were analyzed.

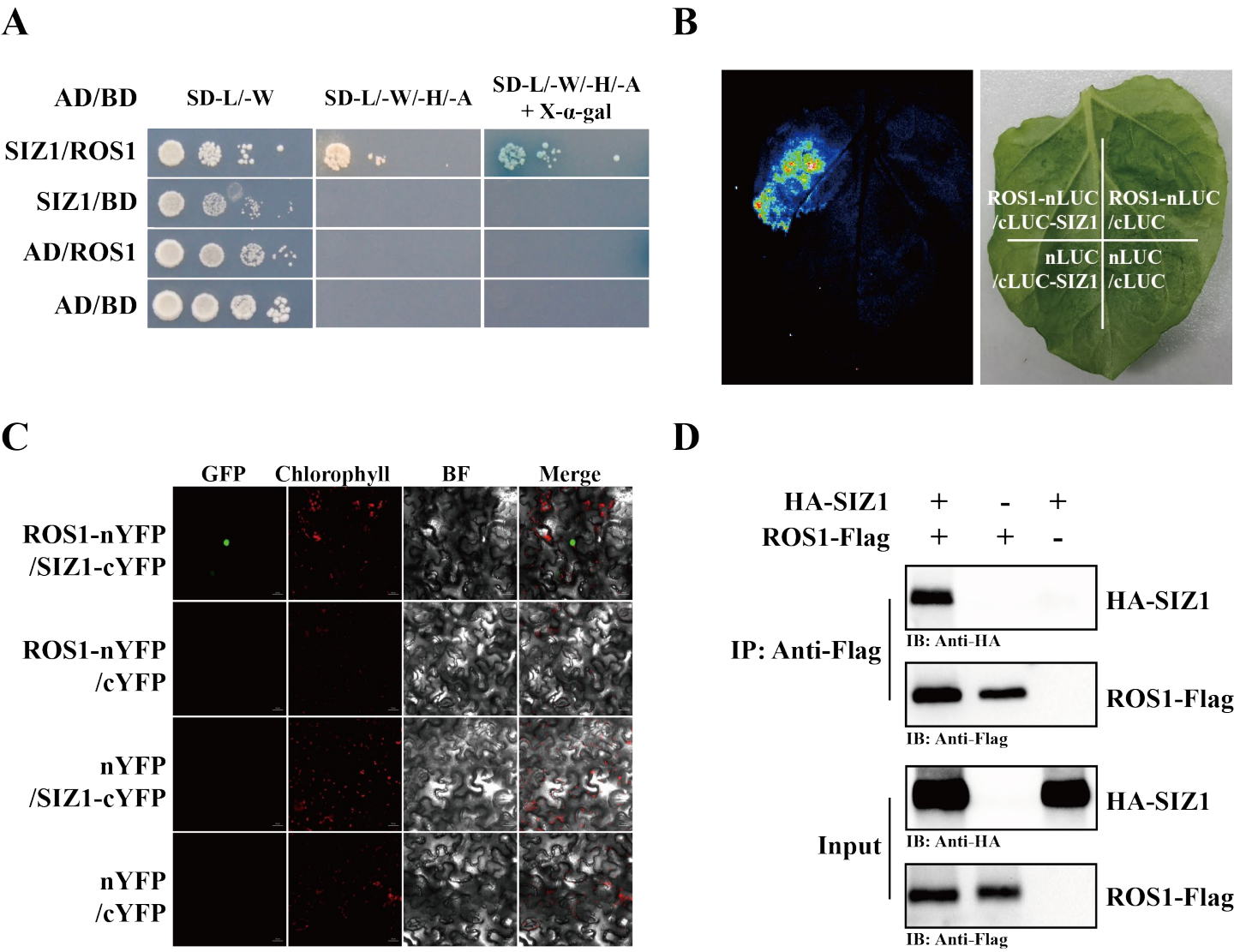

Figure 3. SIZ1 physically interacts with ROS1. (A) Yeast two-hybrid result showing an interaction between SIZ1 and ROS1. Full-length SIZ1 and ROS1 were fused to AD and BD, respectively. The different combination of recombinant plasmids and empty vectors were co-transformed into yeast cells. AD, Gal4 activation domain; BD, Gal4 binding domain. (B) Split-LUC assay showing an interaction between SIZ1 and ROS1 in *Nicotiana benthamiana* leaves. The coding sequences of *SIZ1* and *ROS1* were fused to the C-terminal firefly luciferase and N-terminal firefly luciferase, respectively. (C) Bimolecular fluorescence complementation (BiFC) test indicating SIZ1 interaction with ROS1 in *Nicotiana benthamiana* leaves in the nucleus. Full-length SIZ1 and ROS1 were fused to the C-terminal YFP and N-terminal YFP, respectively. Chlorophyll, the autofluorescence of chlorophyll; BF, bright field; Scale bars, 20 μm. (D) Co-immunoprecipitation showing an association of SIZ1 with ROS1. HA-tagged SIZ1 and Flag-tagged ROS1 were expressed separately or co-expressed in *siz1-2* protoplasts. HA-SIZ1 and ROS1-Flag were detected by immuno-blotting using anti-HA and anti-Flag antibodies with crude lysate proteins and proteins immunoprecipitated via anti-Flag mAb-Magnetic beads, respectively.

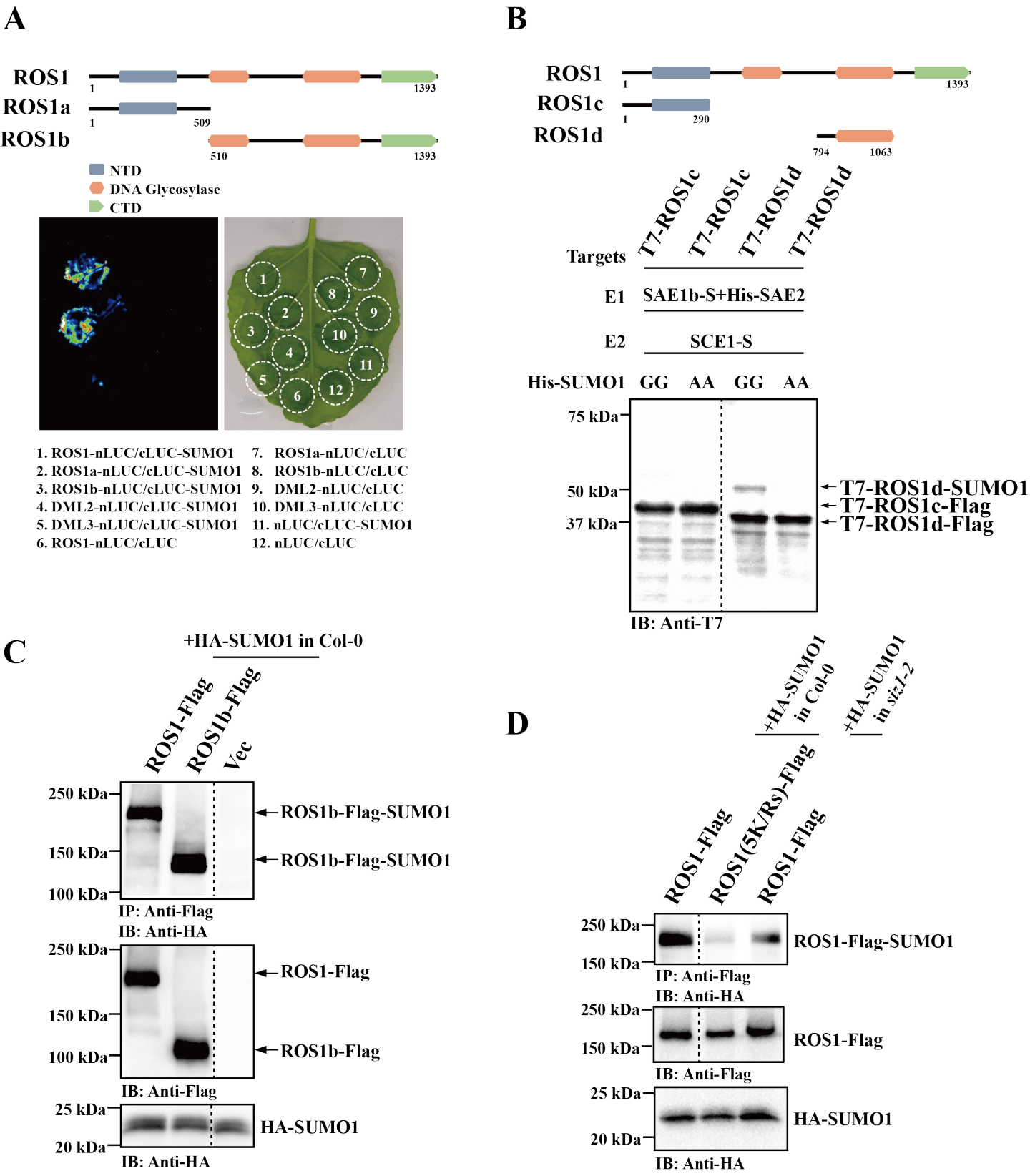

Figure 4. SIZ1 mediates the SUMOylation of ROS1. (A) The interaction of SUMO1 and ROS1 was tested using the split-LUC assay. The C-terminal region of firefly luciferase was fused to the N-terminus of SUMO1. ROS1, DML2 and DML3 were fused to the N-terminal region of firefly luciferase. The schematic diagram shows the full-length ROS1 and the truncated ROS1 (ROS1a: 1-509 aa, ROS1b: 510-1393 aa). NTD, N-terminal domain; CTD, C-terminal domain. (B) SUMOylation of ROS1 was tested using the *Arabidopsis* SUMOylation pathway reconstitution system in *E.coli*. Different combinations of the three plasmids encoding *Arabidopsis* SUMOylation machinery proteins and truncated ROS1 indicated above each lane were co-transformed into *E.coli* BL21(DE3). Immuno-blotting was used to detect truncated ROS1 and its SUMOylated forms using anti-T7 antibody in crude lysate proteins. SUMOylated ROS1 shifting to a larger molecular weight band was observed only in the lane using the mature wild type form of SUMO1 (referred to as SUMO1GG), but not in lanes using mutated form of SUMO1 (referred to as SUMO1AA). The schematic diagram indicates the truncated ROS1 (ROS1c: 1-290 aa (containing K133), ROS1d: 794-1063 aa (containing K806. K812, K851 and K1051)). (C) *In vivo* SUMOylation of ROS1. ROS1-Flag/ROS1b-Flag and HA-SUMO1 were co-expressed in Col-0 protoplasts. The SUMOylated ROS1 was detected via immuno-blotting using anti-HA antibody in proteins immunoprecipitated by anti-Flag mAb-Magnetic beads. Expression of HA-SUMO1 with empty vector served as a negative control. (D) SUMOylation of ROS1 was reduced in *siz1-2*. ROS1-Flag/ROS1(5K/Rs)-Flag and HA-SUMO1 were co-expressed in Col-0 and *siz1-2* protoplasts. SUMOylation of ROS1 was substantially decreased in *siz1-2* compared to in Col-0. SUMOylation in mutant ROS1 with the 5 predicted SUMOylation sites mutated by lysine to arginine substitutions (K133R/K806R/K812R/K851R/K1051R) was reduced.

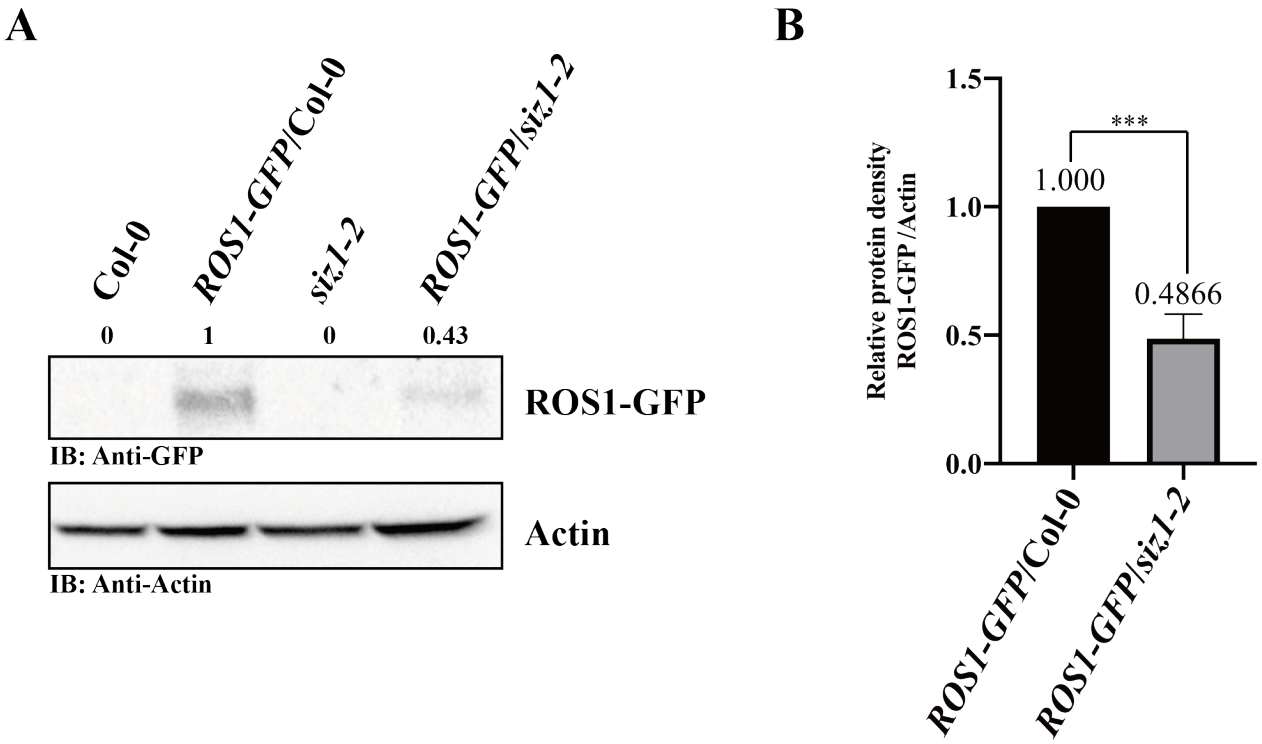

Figure 5. ROS1 protein level is decreased in *siz1-2* mutant plants. (A) Immunodetection of ROS1 protein level by anti-GFP antibody in GFP knock-in lines with GFP integrated in the endogenous ROS1 locus in Col-0 and *siz1-2* background. Col-0 and *siz1-2* without the GFP served as negative controls. Actin detected by anti-Actin antibody was used as a loading control. The protein level of ROS1 relative to Actin shown above the lanes was quantified using Image Lab software (version 5.2.1). (B) Statistical analysis of the ROS1 protein levels in *siz1-2* mutant (n=3). $P = 0.0007 < 0.001$, determined by Student's *t*-test.